ISSN: 2754-4753

Journal of Physics & Optics Sciences

SCIENTIFIC Research and Community

Review Article

Open Access

Laser Ionization Spectroscopy of Atomic Plasma

Ramesh C Sharma[1*], Gagan Sharma[2], Lal Chand Mangal[1], Binoy K Das[1], Vijay K Saraswat[3] and Surya N Thakur[4]

[1]DRDO Electronics and Communication Systems, Facet Range Ramgarh Chandigarh & DRDO New Delhi, 110011 India

[2]Dept of Applied Physics Delhi Technological University New Delhi, 110042, India

[3]Niti Aayog, Science & Technologies, Prime Ministry Office, New Delhi, India

[4]Dept of Physics , Banaras Hindu University Varanasi, 221005, India

ABSTRACT

This study explores the behavior of atomic inert argon (Ar) gases in a normal glow discharge under steady-state conditions using the Laser Opto-Galvanic (LOG) spectroscopic technique. A nickel hollow electrode, connected to a DC voltage source, generates plasma from Ar gases at low pressure inside a Pyrex glass tube. Tunable laser beam is then employed to perturb the steady state of the plasma species electrons, protons, ions, and excited neutral atoms through resonant absorption of the laser light. As the laser wavelength is varied, the signal profile changes over time, with both positive and negative polarity signals recorded. The study also captures spectra for one- and two-photon transitions using a boxcar averager detection system, while adjusting the delay time and gate width. Additionally, the impact of linear and circular polarization on these transitions is investigated. The goal is to present these findings in a clear and accessible way to facilitate understanding among scientists, researchers, and graduate students, promoting further research in the field. A comprehensive atlas of Ar spectral lines in the 400 to 740 nm wavelengths range are created by analyzing the visible spectrum using a pulsed tunable dye laser system. The study identifies the conditions necessary for observing two-photon lines in the optogalvanic spectrum and examines how polarized light affects the relative intensity of these lines. The temporal evolution of the optogalvanic signals is also tracked. A theoretical framework for the experimental work is provided, shedding light on the underlying mechanisms of the Opto Galvanic Effect (OGE). Finally, the study discusses the use of OGE in calibrating spectroscopic instruments, spectrum detectors, and opto-electronic devices.The technique has important applications in fields such as combustion diagnostics, isotope separation, Rydberg series analysis, micro/nanoelectronics production, and plasma physics.

***Corresponding author**

Ramesh C Sharma, DRDO Electronics and Communication Systems, Facet Range Ramgarh Chandigarh & DRDO New Delhi, 110011 India.

Received: September 10, 2025; **Accepted:** September 17, 2025; **Published:** November 20, 2025

Keywords: Ionization Spectroscopy, Optogalvanic Effect, Two Photon Transitions, Polarization Effect

Introduction

The OGE induced by lasers in steady gas discharge is the focus of this investigation. A pivotal study by Green and colleagues in 1976 highlighted the remarkable sensitivity of LOG spectroscopy using a dye laser with variable wavelengths, significantly increasing interest in this technique [1]. Since then, Schenck et al. have utilized the OGE to monitor atomic ions and explore molecular transitions in discharges and flames [2]. The OGE has also been applied in two-photon spectroscopy and in the Doppler-free technique of saturation spectroscopy, and it has been proposed as a potential method for isotope separation. The OGE is expected to be valuable as a diagnostic tool for the kinetic analysis of flames and discharges. Suzuki et al. have extensively applied this technique to study atomic and molecular species in microwave and radiofrequency-induced discharge plasmas [3]. LOG spectroscopy serves as an alternative to fluorescence absorption methods, as the disturbance of discharge characteristics caused by laser light is typically minimal even at high saturation levels, allowing the opto-galvanic effect to be considered directly proportional to the number of absorbed photons. The current study aims to systematically examine the LOG spectrum associated with the visible electron transitions of argon [4-12]. It specifically seeks to investigate the intensity of the LOG signal in relation to the adjustable wavelength of interest.

The LOG spectrum of argon will be analyzed using pulsed Nd laser-pumped tunable dye lasers in the visible range. The objectives of this work are to:

- Create a comprehensive atlas of argon's opto-galvanic spectral lines in the visible region.
- Identify the conditions under which two-photon lines of argon are observed in the LOG spectrum.
- Examine the effect of polarized light on the relative intensities of the two-photon lines.
- Understand the temporal evolution of the opto-galvanic signals.

Opto-Galvanic Effect

When a discharge is illuminated with radiation whose wavelength corresponds to an atomic or molecular transition, the electrical impedance of the discharge changes; this phenomenon is known as the opto-galvanic effect (OGE).

In a stable normal glow discharge operating at a specific DC voltage, neutral molecules in the discharge tube are distributed across various energy levels, including the ground state (Figure 1). A low-density plasma of ions and electrons is also present. When

a laser beam is directed through this discharge, and its frequency matches the energy difference between two atomic (or molecular) levels one or both of which are populated the population distributions in these energy levels are disturbed. This disturbance leads to a shift in the discharge impedance, which can be detected by changes in the discharge voltage or current. This change is referred to as the laser opto-galvanic signal [5].

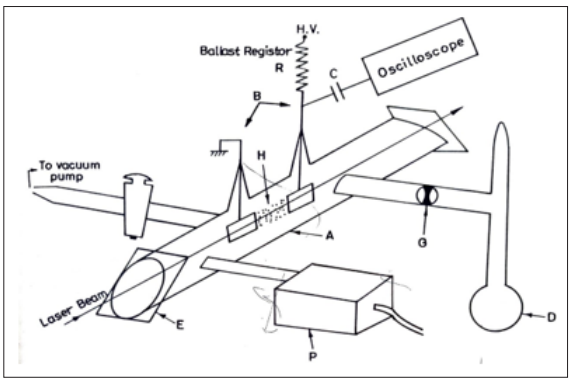

Figure 1: Schematic Diagram of an OG Cell.

A-Pyrex glass cell, B – Nickel electrodes, P -Pirani gauge, D -Sample holder, E- Quartz window, G-Needle valve, H -Discharg.

As illustrated in Figure 2, the continuous glow region of an electric discharge is defined by the constant current (I) and the constant voltage drop (V) maintained between the electrodes. These two factors establish the static current-voltage characteristics of both the sustaining DC power supply and the electric discharge in the plasma. A self-sustaining discharge occurs when the DC potential (V) across the two electrodes, in series with a current-limiting resistor (R), exceeds the breakdown voltage. In this phase, secondary ionization takes place when a primary electron generated externally gains enough energy from the electric field to collide with other particles. Consequently, the discharge can continue even if the external ionization source is turned off. At low currents around (10-6) amps, the discharge is characterized by a constant voltage and no light emission, a condition known as a dark discharge or "Townsend discharge." As the current increases, space charge effects lead to a cathode voltage drop. Before stabilizing at a constant value (V), the voltage decreases through a transitional region known as a subnormal low discharge. This state is typically referred to as a normal glow discharge, resulting in a visible glow. The cathode fall potential, which is approximately 200–300 V and remains relatively constant for currents ranging from 1 to 100 mA, is only slightly exceeded by the voltage.

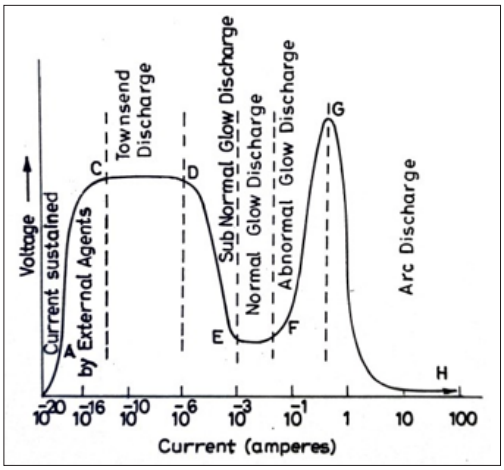

Figure 2: Schematic of a Gas Discharge between Flat Parallel.

A glow discharge is defined as a phenomenon in which the cathode emits electrons while being bombarded by particles and light from the gas. The positive space charge primarily shapes the electric field near the cathode. To maintain the discharge, thermal effects are either minimal or not essential. The term "glow discharge" describes a bright region that forms close to the cathode, separated from it by a darker area.

Figure 3 shows how the visible light emitted by a direct current glow discharge is distributed along a long cylindrical tube filled with a rare gas at a pressure of 0.1 to 1 mm Hg. There may be a very thin black region (Aston's dark space) at the cathode, followed by the cathode glow a thin, relatively faint luminous layer before reaching the cathode dark space. The cathode glow and Aston's dark space are not always easily visible. A distinct boundary separates the cathode dark space from the negative glow, which gradually diminishes as one approaches the "Faraday dark space." Additionally, a dark space and glow may occasionally be observed at the anode end of the positive column.

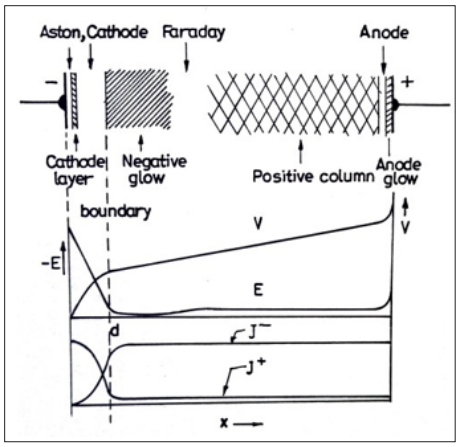

Figure 3: Spatial Distribution of Dark and Luminous Zones: Electric Field (E), Potential (V), and Current Densities (J+ and J -) in a Glow Discharge.

Hollow Cathode Discharge (HCD)

The hollow cathode is a distinct type of glow discharge contained within an open-ended metallic cathode cylinder that faces a small anode situated about one centimeter away along its axis [13,14]. The cell housing both electrodes can be evacuated and filled with the necessary gases and vapors at a pressure of a few m-Torr. A voltage of approximately 200 volts is applied across the electrodes. This discharge produces an exceptionally bright glow that fills the interior of the cathode, accompanied by an annular dark region near the inner wall. Hollow cathode discharge (HCD) tubes have been widely used in optogalvanic spectroscopy research, with various theories regarding HCD discussed in the literature [15,16]. In this study, we will utilize a Fe-Ar hollow cathode lamp (L233-Fe) from Hamamatsu Photonics (Japan), which operates at a voltage range of 180 to 200 volts.

Mechanism of LOG Signal Generation

When a discharge tube is illuminated with laser light, its impedance can vary around its steady-state values, resulting in both positive and negative signals. Three main models have been proposed to explain the behavior of the LOG signal: the temporal profile model, the ionization model, and the electron temperature model. The following sections provide a brief overview of each of these models.

Ionization Model

The ionization model has been developed by both Smyth et al, as well as Drouet and Novak [17-19]. This model describes a weakly ionized, self-sustaining plasma composed of neutral species, ions, and electrons when exposed to a strong laser beam. The laser's frequency may align with the energy differences between two ions, molecules, or energy levels. This resonance leads to a change in the ionization rate, disrupting the steady-state population of the relevant levels through upward or downward transitions.

Case 1

The ionization rate of atoms or molecules from this state due to collisions with electrons would be greater if the upper energy states had a longer lifetime than the lower states. In this scenario, laser irradiation reduces the discharge's impedance by increasing the number of available electrons and ions. This leads to:

a. A negative voltage LOG signal.
b. A positive LOG signal in terms discharge current.

Case 2

Although the likelihood of ionizing an atom or molecule in a higher energy state is generally greater, the ionization rate effectively decreases if the upper excited state is short-lived compared to the lower state, resulting in an increase in discharge impedance. This leads to:

a. Positive voltage LOG signal.
b. Negative voltage LOG signal

Case 3

If the life time of the two-state involved are of the same order then we get positive or negative OG signal depending upon whether the laser beam irradiation finally results in an increase or decrease of ionization rate.

Electron Temperature Model

The incident light energy absorbed by the atoms or molecules in the discharge can be rapidly transferred to the electron gas through a super elastic collision. This transfer raises the electron temperature, which in turn increases conductivity, reducing discharge impedance and increasing discharge current. The signal is mainly influenced by the stimulated energy level and the rate at which energy is transferred to the electron cloud. The findings of Dreze et al, can be explained by the transfer of excitation to the electron gas, followed by the redistribution of energy among all species due to collisions with electrons [20].

Experimental: Instrumentation and Techniques

A spectroscopic experiment typically requires an excitation source, a basic cell, and a detector with strong signal-to-noise discrimination capabilities. To enhance weak signals that may be masked by noise, the detection system in experiments using a laser as the excitation source primarily employs electronic circuits. The gated detection technique utilizing a boxcar average has been extensively used in the experiments presented in this thesis. While this method effectively reduces noise, optimizing the design of the sample cell and the electronic circuits for preamplification can further enhance the performance of the detection system.

A lens with a focal length of 20 cm is used to focus a small portion of the dye laser beam onto the Fe-Ne hollow cathode lamp. The LOG signal from the Fe-Ne (Hamamatsu Model L233-Fe) hollow cathode lamp is received by the second boxcar integrator (EG&G Model-164), which has an input sensitivity of 100 mV. After configuring the gated integrator's time constant to 1.0 μs, the processed signal is transmitted to the second pen of the strip chart recorder [21,22].

Figure 4 illustrates the experimental setup for argon LOG spectroscopy. The Fe-Ar Hamamatsu (Model L233-Fe) lamp receives a concentrated portion of the laser light pulses from a Nd-YAG pumped dye laser. A lens with a focal length of 15 cm is used to focus the laser beam into the lamp. It was found that two-photon transitions can only be observed with precise focusing. A high-voltage, stable power supply (Keithley Model 246) applies a voltage in the range of 180–200V to the cathode through a current-limiting resistor of 2.5K. A 5 μF capacitor is employed to extract the signal generated in the lamp, which is then sent to the boxcar integrator for processing.

The second portion of the beam is focused onto a Fe-Ne hollow cathode lamp through a 10K ballast resistor, with a voltage applied between 160 and 200V from a high-stabilized power supply (Bertan Model 125, USA). A 0.1 μF capacitor is used to extract the

LOG signal generated in the lamp, which is then sent to a second boxcar averager (EG&G Model 164) for wavelength calibration. By scanning the dye laser wavelength, we can display the argon spectra alongside the calibration Ne spectrum. We recorded one- and two-photon argon spectra using three different laser dyes: LDS-730 (740-720 nm, Region I), LDS-698 (720-670 nm, Region II), and DCM (670-675 nm, Region III). The dye laser radiation had a spectral bandwidth of 0.2 cm^{-1}, with pulse energies of 35 mJ in Region I, 70 mJ in Region II, and 45 mJ in Region III. The laser was pumped by the Nd-YAG laser's 532 nm radiation, which provided an energy of 250 mJ per pulse.

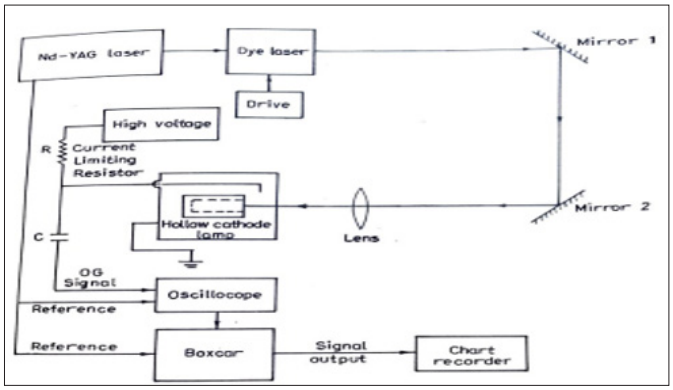

Figure 4: Schematic Diagram of the Experimental setup for Recording the LOG Spectrum of Ar.

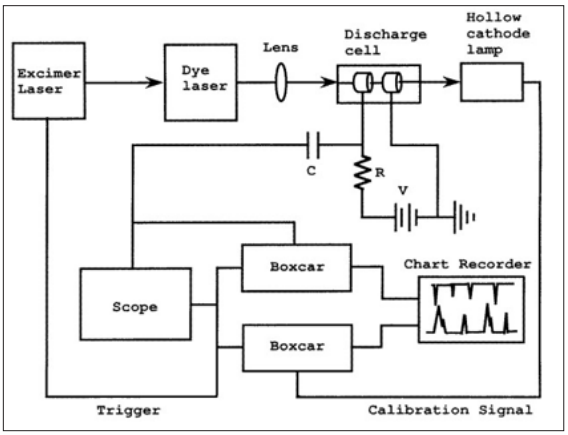

Figure 5: A Schematic Diagram of the Experimental Set-Up.

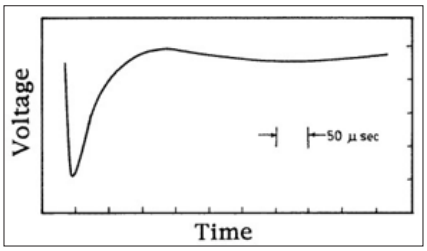

Figure 6: A Typical Oscilloscope Trace of the Two-Photon LOG Voltage Signal of the Argon-Filled Discharge Cell.

Spectroscopic Analysis

LOG Spectroscopy of Ar gaseous discharge have been studied by Sharma and Thakur et al. The ground state of A r as for all other rare gas atoms is a 1S0 corresponding to the closed shell electronic configuration 1s22s22p63s23p6 [21, 22]. In the first excited electronic configuration one of the 3p6 electrons is excited to the 4s shell and the four resulting levels were empirically designated as 1s2,1s3,1s4and 1s5 in the order of decreasing energy of excitation [21,23]. The second group of excited energy levels resulting from the electronic configuration 1s22s22p63s23p54p1 are ten in number and empirical Paschen notation for them in the order of decreasing excitation energy is 2p1,2p2,2p3…… 2p10. The third group excited energy levels of Ar result from the electronic configuration 1s22s22p63s23p53d1 and their number is twelve. The ground state 1S0 of Ar lies much deeper than any of the odd parity excited state and allowed transitions between the ground and higher states lead to series of lines in the vacuum UV.

The L-S coupling approximation is nearly valid for the first excited configuration 3p54s1 and by Hund's rules the four terms in the order of increasing energy are 3p2,3p1,3p0 and 1p1. The transitions between 1p1 and the ground state is allowed where as those to the remaining three excited states forbidden to different extents on the basis of ΔS and ΔJ selection rules. In the electronic discharge Ar atoms are excited to the various higher energy states and its emission lines in the visible region generally correspond to transitions between pairs of excited energy states. LOG effect in Ar discharge consists of changing the population distribution of atoms in the excited states when the incident laser radiation is resonant with a pair of such states. The change in population distribution leads to a change in the rate of ionization and hence either an increase or decrease of the macroscopic impedance of the gas discharge. Using a wavelength tunable dye laser, the voltage changes or current change in the electric circuit involving the discharge tube is monitored and this forms the LOG spectrum of the Ar atoms. The analysis of the spectrum requires a detailed knowledge of the atomic states resulting from different electronic configuration. These aspects are discussed in the following sections.

Spectroscopic Notations

The L-S coupling is not a satisfactory scheme to designate excited energy levels of Ar atom and in the present work we have followed the J-1 coupling scheme first suggested by Racah [24]. In the theJ-1 coupling scheme we start from the singly ionized Ar atom with electronic configuration 3p5 which gives the inverted energy states $^2p^0_{3/2}$ and $^2p^0_{1/2}$. The superscript "0" refers to the odd parity of these states resulting from $\sum 1_i$ =odd where 1_i refers to the orbital angular momentum quantum number of the ith electron. The excited states resulting from the configuration $3P^5 4s$ are obtained by considering the j values of the two states of singly ionized Ar atom and then adding vectorially the l value of the 4s electron. The vector sum of $J\perp\!\!\!\rightarrow$ and $l\perp\!\!\!\rightarrow$ is represented by$K\perp\!\!\!\rightarrow$ where the quantum number K can be take all half integral values between |j+l| and |j-l| The total angular momentum $J\perp\!\!\!\rightarrow$of the resulting atomic state is given by the vector sum of $K\perp\!\!\!\rightarrow$ and $S\perp\!\!\!\rightarrow$ where $S\perp\!\!\!\rightarrow$ represents the spin angular momentum ½ h of the electron. The atomic state is designated by [K]^p J where 'p' stands for parity and is replaced by 'o'for states and this superscript is dropped for even states.

For the configuration 3p54s we have two sets of states corresponding to $[^2p^0_{3/2}]4s$ and $[^2p^0_{1/2}]4s$.

For $[^2p^0_{3/2}]4s$, k=3/2, s=1/2 so that J=2 and 1 and energy states are [3/2]°2 and [3/2]°1.

For $[^2p^0_{1/2}]4s$, k=1/2,s=1/2 and J=1 and 0 leading to the states 4s'[½]°1 and 4s'[1/2] °0.

The complete set of the excited states resulting from 3p54s configuration is

4s[3/2] °2, 4s[3/2]°1, 4s'| 1/2]°1 and 4s [1/2] °0

Where 'prime factor' to the states resulting from the ionic state [2p01/2] and those without prime result from [2p03/2] state of

the ion.

The ten excited states originating from the electronic configuration 3p54s are designated as follows:

For [2p3/2]4p:

K=5/2,3/2 and 1/2 leading to the following six states when $J=K\perp\rightarrow+S\perp\rightarrow$ is considered.

4p [5/2]3, 4p [5/2]2, 4p [3/2] 2, 4p [3/2]1, 4p [1/2] 1 and 4p[1/2]0.

$[^2p^0_{1/2}]4p$

K=3/2, and 1/2 and four states arising from this arrangement are 4p' [3/2]2, 4p' [3/2]1, 4p' [1/2]1, 4p' [1/2]0.

It is to be noted that all these states have been parity. In a similar way the twelve excited states originating from the electronic configuration 3p53d are

For $[^2p^0_{3/2}]3d$

K=7/2,5/2,3/2,1/2 leading to eight states 3d [7/2] °4, 3d [7/2] °3, 3d [5/2] °3, 3d [3/2] °2, 3d [3/2] °1, 3d [1/2] °1, 3d [1/2] °0.

For $[^2p^0_{1/2}]3d$:

K=5/2 and 3/2 which gives rise to four states 3d' [5/2]°3. 3d' [5/2]°2, 3d' [3/2]°2, 3d' [3/2]°1.

One photon transition are allowed only to the excited states of parity subject to the restrictions imposed by ΔL and ΔJ selection rules. When intense laser beam is incident on the argon discharge all simultaneous absorptions of two photon may occur resulting in spectral lines which are not observed under electric discharge excitation.

Selection Rules

One photon transition in Ar are governed by electric dipole selection rule which requires that:

(1). Transition occurs between energy states of opposite parity that is

odd↔even,odd↔odd,even↔even

2. $|J_e-J_g|=0,\pm1$

$J_e=0\leftrightarrow J_g=0(\Delta J=0,\pm1)$

where subscript e and g stands for upper and lower states respectively.

The two photon transition depend on the value of matrix element of the symmetrical operator $Q_{\varepsilon1,\varepsilon2}$ between levels e and g, where ε1 and ε2 represent the polarization states of the two-photon which simultaneously interact with the atom. If the value of matrix element is zero there is no two-photon transition.

$Q_{\varepsilon1,\varepsilon2}$ is symmetrical with respect to exchange of the two polarizations if the two photons propagates in the same or opposite direction have the same frequency. If the two-photon have different frequencies, it is necessary to define another operator which is not always symmetrical. $Q_{\varepsilon1,\varepsilon2}$ may be decomposed into the scalar operator(tensor of rank 0) and a quadrupole operator (tensor of rank 2) and leads to the following selection rule for the angular momentum of atom.

$J_e\text{-}J_g\leq2,J_\alpha=0\leftrightarrow J_\beta=1(\alpha,\beta=e,g\vee g,e)$

$(\Delta J=0,\pm1,\pm2)$

The parity of the upper and lower states must be the same which requires

odd↔even,odd↔odd,even↔even

The two photon transitions connect those atomic levels which cannot be reached by one photon transitions.

Results and Discussion

The first reported logarithmic (LOG) spectrum of the Argon (Ar) atom, as documented by Nestor, was obtained by irradiating miniature glow discharge lamps with a pulsed, tunable dye laser in the wavelength range of 695-795 nm [25]. Within this region, only three spectral lines exhibiting a negative LOG signal were observed. M.-C. Su et al. explored the use of the Ar LOG spectrum for wavelength calibration of dye lasers, specifically in the Nd:YAG laser-pumped Rhodamine 6G dye laser region (555-575 nm), identifying 36 electronic transitions that were highly suitable for this purpose [26]. Penning-type ionization energy transfer collisions in an Ar-Hg discharge were detected in the LOG spectrum by Reddy et al. [27].

The temporal evolution of LOG signals was investigated in detail in Fe-Ne and Ar-Hg discharges by irradiating them with excimer-pumped dye lasers. Notably, the spectral lines at 4510.7 Å ($1s^2$-$3p^5$), 4596 Å ($1s^2$-$3p^7$), and 4628.4 Å ($1s^2$-$3p^8$) exhibited identical shapes and displayed characteristic anomalous signal behavior. This was attributed to the exchange of excitation energy between Ar and Hg atoms [28-36]. The $3p^1$ state of mercury participates in energy transfer collisions, which leads to the ionization of Hg atoms, while simultaneously causing the Ar atom in the $1s^2$ state to relax to its ground state.

Reddy et al. also investigated the LOG spectrum of Ar in the visible wavelength region (415-670 nm) by axially irradiating a hollow cathode discharge lamp with a tunable dye laser pumped by an excimer laser [29]. These studies identified 180 atomic lines from electronic transitions, all of which were attributed to single-photon transitions, as per the assignments of Reddy et al., using the j-1 coupling scheme proposed by Racah [24,27]. Furthermore, LOG spectra in the wavelength regions of 500-5300 Å and 6010-6700 Å were also studied by Reddy et al. Murnick et al. investigated LOG signals at 667.7, 751.5, and 696.5 nm from the $3p^1$ and $3p^2$ levels of the Ar atom in a discharge setup, revealing unexpected signal behaviors and time dependencies [29,30]. These results were interpreted as the result of radiative trapping effects and collisional mixing between resonance and metastable levels.

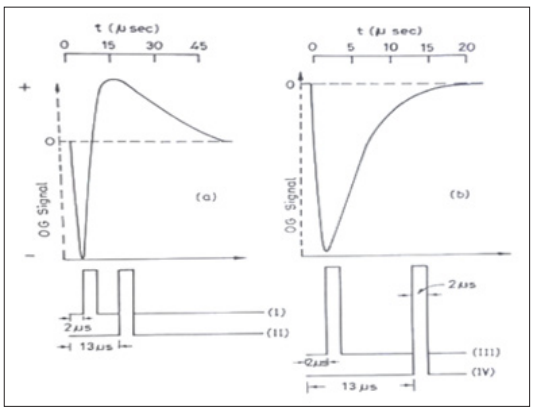

Figure 7: Temporal Evolution of the LOG Signals at (a) 13988.3cm-1 and (b) 14008.8cm-1 in the Ar Discharge.

Extensive studies of the neon (Ne) atomic logarithmic (LOG) spectra have provided significant insights into both one-photon and two-photon transitions [30-33]. Sharma et al. were the first to record two-photon LOG transitions in an argon (Ar) discharge using a Nd:YAG laser-pumped dye laser, with excitation via both linearly and circularly polarized laser radiation in the wavelength range of 605-740 nm (16516-13523 cm^{-1}) [21,22]. They also investigated the theoretical intensity ratios for these transitions. Additionally, one-photon excited optogalvanic transitions in this region were documented, many of which were reported for the first time, highlighting their potential as calibration standards.

The temporal profiles of the LOG signals at various wavelengths revealed that these signals could be categorized into two distinct types. The second group of transitions exhibited a voltage profile characterized by a negative voltage signal, observed both with a short boxcar gate delay and with a longer gate delay relative to the excitation laser pulse. Conversely, the first group of transitions showed a negative signal at short gate delay times and a positive signal at longer delay times. The voltage profiles for the two groups of transitions, along with the corresponding boxcar gate delay after laser excitation, are schematically presented in Figure 7.

Description of the LOG Signal in Argon Hollow Cathode Discharge Sharma et al. pulsed Nd-YAG laser pumped tunable Dye LOG spectra have been studied and monitored on a oscilloscope and simultaneously processed by a boxcar average, both units were triggered by a photodiode receiving a small fraction of the incident Nd-YAG laser pulse [21,22]. A general survey of the temporal profile of the signals at several wavelength showed that they could be grouped into two types. The first group of optogalvanic transition exhibit a composite voltage profile which starts with the negative voltage signal, becomes minimum after about 2 μs then increase to a maximum positive voltage after 10-15 μs and asymptotically decrease to 0 at the end of 50 μs is given (Figure 8a). the second group of transitions exhibit a negative voltage profile with minimum 2 μs from the excitation laser pulse and asymptotically increase to 0 after about 20 μs (see Figure 8b). the boxcar processed LOG signal were recorded on a chart recorder with the dye laser grating scan rate of 0.3 nm/min.

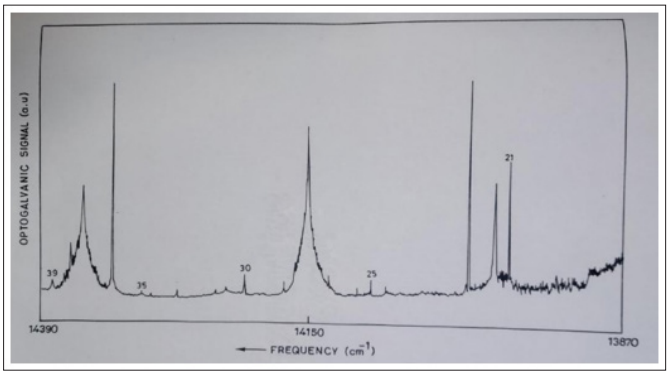

Figure 8a: LOG Spectrum of Ar in the Frequency Region 13870 to 14390 cm-1.

The LOG spectrum shown in Figures 9 in the frequency region 13976-14803cm-1(720-670nm) and 14925-16516cm-1(670-605nm) of the LDS-698 & DCM dyes region II and III were recorded with the boxcar gate delay of 2 μs & 4 μs respectively. Similarly we also observed optogalvanic transitions in the wavelength range (720-740nm) of LDS-730 dye region I [see Table 2]

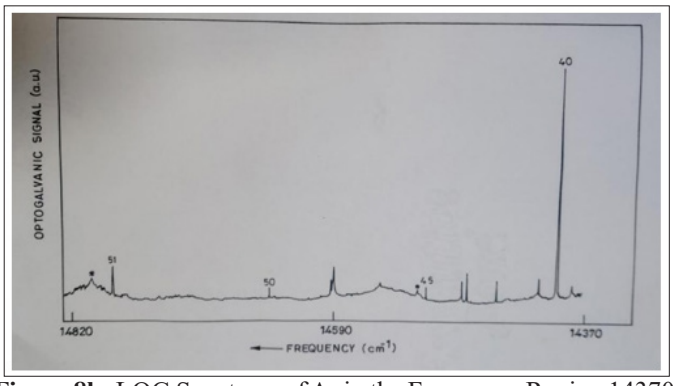

Figure 8b: LOG Spectrum of Ar in the Frequency Region 14370 to 14820 cm^{-1}.

Figure 9 shows the LOG spectra in the frequency region 13950-14400cm-1 (717-694nm) recorded with the boxcar gate width of 2 μs and at two different gate delays from the exciting laser pulse 2 μs and 13 μs. It is seen from Figure 9a (gate delay 13 μs) and 9b (gate delay 2 μs) that the relative negative voltage signal for the second group of LOG transitions are greatly diminished, for the longer boxcar delay [Figure 9a] and the LOG signals for the first group becomes positive in polarity. It was found that the maximum number of argon lines (all with the negative voltage signals) in any dye laser region could be simultaneously recorded by setting the boxcar gate delay 2 μs [see Figure 9c]

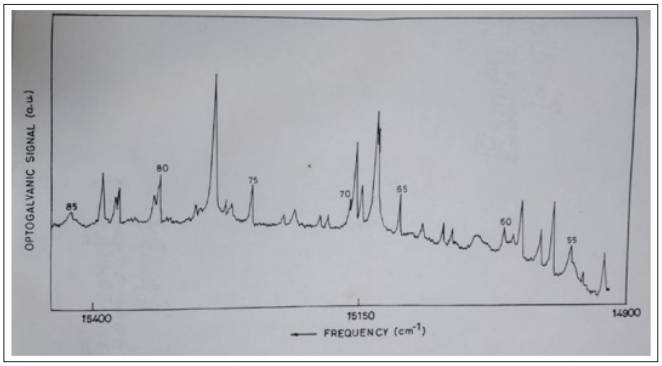

Figure 9a: LOG Spectrum of Ar in the Frequency Region 14900 to 15400 cm^{-1}.

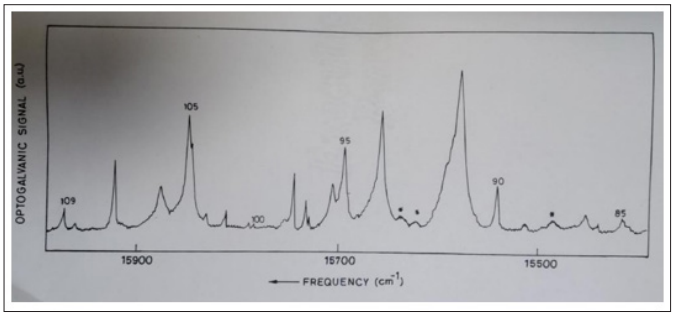

Figure 9b: LOG Spectrum of Ar in the Frequency Region 15400 to 15900 cm^{-1}.

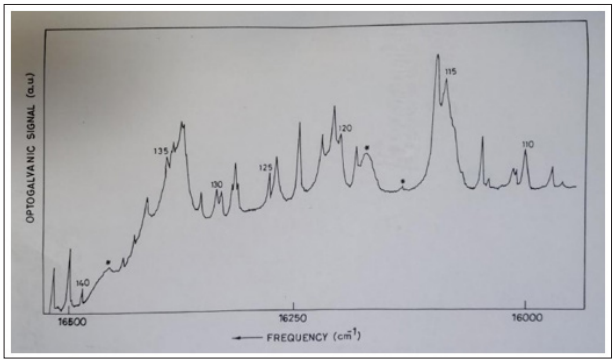

Figure 9c: LOG Spectrum of Ar in the Frequency Region 15900 to 1650cm^{-1}.

Spectroscopic Assignments

The frequencies of the observed spectral lines were determined by fitting a second degree polynomial to the measured line position, with a maximum uncertainty of 1.0 cm^{-1} these are given in the second column of Table 1The relative optogalvanic intensities (estimated from peak height for linearly polarized light) are given in the third column but these are not normalized for the spectral power variations of the dye laser output and in the case of overlapping transitions the relative intensities in the two dye regions are also shown (within bracket).The upper and lower energy levels of the transition, in Racah notation, are given in the fourth and fifth columns respectively and the transition type (one or two photon) is shown in the sixth column [24]. In Region II, the relative intensities of two-photon transitions were also determined for circularly polarised light and the ratio (Ω) of circular to linear polarisation intensities is included in the sixth column along with the corresponding uncertainty. Thespectroscopic assignments are quite straight forward in terms of the known energy levels of argon and all, except eight of the 142 [29]. Observed lines have been satisfactorily assigned (see Table 1). Some of the observed lines have two assignments within the limit of uncertainty.

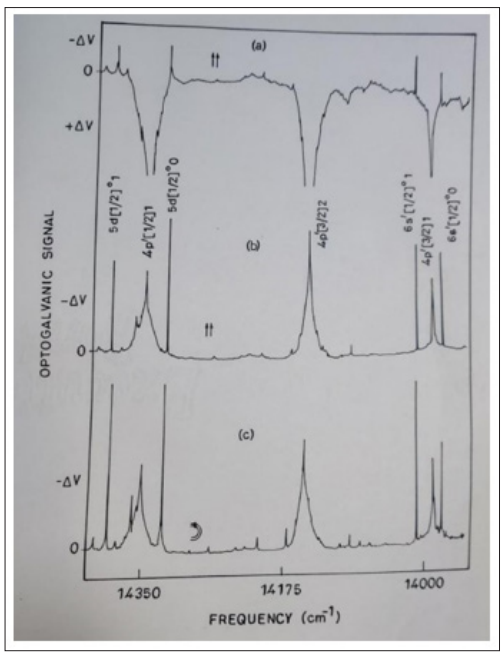

Figure 10: LOG Spectrum of Ar using Polarised Laser Radiation with a Boxcar Gate Delay of (a) 13μs (Linear Polarization) (b) 2μs (Linear Polarization) (c) 2 μs (Circular Polarization).

The metastable 4s[3/2]°2 level accounts for more than half of the 43 two-photon resonant transitions whereas 10 of them originate in 4s [3/2]°1 four in 4s' [1/2]°0 and only two in 4s' [1/2] °1 1evel. A partial energy level diagram of Ar is given in Fig. 20 to explain the origin of some very intense spectral 1ines. The intensities of two-photon optogalvanic transitions are very sensitive to changes in incident laser power, unlike the one photon transition. The strongest two photon lines are observed at 13976.6, 14008.8 and 14324.9, 14393.7 cm -1 centred around strong one photon transitions at 13988.3 and 14352.7 cm-1 respectively, all of them originating in the 4s [3/2]°2 level. The relative intensities of these transitions under linear and circular polarizations are shown in Fig. 10(b) and 10(c) respectively and discussed in the next section.

Only nine of the one-photon transitions have metastable states as their lower energy levels [See Region II of Table 1]: the three originating in 4s[3/2]°2 are very strong and are probably power broadened due to high laser intensity [see Figure 11], while those originating in 4p[5/2]3, s4p' [1/2]1 and 4p[1/2]1 give rise to medium strong LOG signals. All the 81 limits of uncertainty. photon transition. The strongest two photon lines are observed at centred around strong discussed in the next section. One-photon optogalvanic transitions in Region I and Region II and many of them in Region III have been observed for the first time; for some of the transitions in Region III reported earlier we have noticed printing or assignments errors (marked** in Table 1) [29]. As can be seen from Table 1, 4p [3/2]2, 4p[3/2]1 and 4p [5/2]2 form lower levels of many one photon transitions whereas 4p[5/2]3 and 4p (1/2] 1 are associated with two very strong LOG signals each.

Grynberg et al. and Sharma et al. have carried out a detailed analysis of optogalvanic intensity, arising from the scalar and the quadrupolar components of the two-photon transition tensor for Doppler-free two-photon spectrum of neon [21,22,37]. They conclude that the experimental observations on polarization characteristics do not agree with theoretical prediction unless one makes use of accurate wavefunctions for the initial, final and various intermediate states. We also qualitatively account for the observed ratio (Ω) in the following way. We have calculated the optogalvanic intensity ratios of circular to linear polarized light (Ω = circular/linear) by evaluating the contributions of scalar and quadrupolar components using the two-photon matrix given by [37,38];

$$r_g = \frac{A}{2J_g+1}\sum_{k=0,2}\frac{\left|\langle eJ_e||Q^k||gJ_g\rangle\right|^2}{2k+1}\left(\sum\left|a_q^k(\varepsilon_1,\varepsilon_2)\right|^2\right)$$

$$= \frac{A}{2J_g+1}\left[\frac{\left|\langle eJ_e||Q^0||gJ_g\rangle\right|^2}{1}(|a_0^0(\varepsilon_1,\varepsilon_2)|^2) + \frac{\left|\langle eJ_e||Q^2||gJ_g\rangle\right|^2}{5}\left(\sum\left|a_q^2(\varepsilon_1,\varepsilon_2)\right|^2\right)\right] \quad (15)$$

Where ε_1 and ε_2 represent identical polarizations for the two photons. Using

$$|a_0^0(\varepsilon_1,\varepsilon_2)|^2 = {}^1/_3$$
$$\sum\left|a_q^2(\varepsilon_1,\varepsilon_2)\right|^2 = {}^2/_3 \quad \text{for linear polarization} \quad (16)$$

$$|a_0^0(\varepsilon_1,\varepsilon_2)|^2 = 0$$
$$\sum\left|a_q^2(\varepsilon_1,\varepsilon_2)\right|^2 = 1 \quad \text{for circular polarization} \quad (17)$$

We get,

$$\Gamma_{g(circular)} = \frac{A}{2J_g+1}\left[\frac{\left|\langle eJ_e||Q^2||gJ_g\rangle\right|^2}{5}\right] \quad (18)$$

$$\Gamma_{g(linear)} = \frac{A}{2J_g+1}\left[\frac{1}{3}\frac{\left|\langle eJ_e||Q^0||gJ_g\rangle\right|^2}{1} + \frac{2}{15}\frac{\left|\langle eJ_e||Q^2||gJ_g\rangle\right|^2}{5}\right] \quad (19)$$

And hence

$$\Omega = \frac{\Gamma_{g(circular)}}{\Gamma_{g(linear)}} = \frac{1/5C}{1/3B + 2/15C} \quad (20)$$

Where

$$B = \left|\langle eJ_e||Q^0||gJ_g\rangle\right|^2$$

$$C = \left|\langle eJ_e||Q^2||gJ_g\rangle\right|^2$$

The following derivations of Ω are valid only when there is only one intermediate real level with energy close to that of one photon.

Case 1. When J_e is different from J_g then $\left|\langle eJ_e||Q^0||gJ_g\rangle\right|^2 = 0$

so that

$$\Omega = \frac{1/5}{2/15} = 1.5 \quad (21)$$

Case 2. When J_e is equal to J_g and greater than or equal to 1, then

$$R = \frac{\left|\langle eJ_e||Q^0||gJ_g\rangle\right|^2}{1/5\left|\langle eJ_e||Q^2||gJ_g\rangle\right|^2} = \frac{B}{1/5C}, \quad (22)$$

where R is the ratio of scalar to quadrupolar components, the value of R has been calculated from the Racah coefficients according to the following relation:

$$R(g,e,J_r) = \frac{1}{3(2J_g+1)\begin{bmatrix} J_e & J_g & 2 \\ 1 & 1 & J_r \end{bmatrix}^2}$$

$$R=1 \text{ if } J_e=J_g=1; R=3 \text{ if } J_e=J_g=2 \quad (23)$$

where J_e is the angular momentum of the real intermediate level. Now from eqs (20) and (22), Ω is given by

$$\Omega = \frac{1/5}{1/15R + 2/15}$$

$$\Omega = 1 \; if \; R = 1; \Omega = 0.6 \; if \; R = 3 \quad (24)$$

The observed values of Ω for transitions at 14471.7 cm $^{-1}$ and 14648.7 cm $^{-1}$ as shown in table 2 are in good agreement with the calculated value of 0.6 corresponding to transitions between two levels with J' = J" = 2. Similarly, the observed values of Ω for transitions at 14365.0 cm $^{-1}$ and 14382.0 cm $^{-1}$ agree well with the calculated value of 1.0 corresponding to transitions with J'= J" = 1. However, the calculated value of ft for transitions corresponding to J'≠ J" do not agree with the observations except for that at 14393.7 cm $^{-1}$ with Ω = 1.5 ±0.1 compared to the theoretical value of 1.5. Thus, it is found that a single intermediate level approximation is not very successful in the calculation of Ω for two photon transition intensities between levels with unequal J values.

The enormously large intensity of two pairs of two-photon transitions must be due to the near resonance intermediate state. The 4p'[3/2]1 level is almost halfway between the 6s'[1/2]°1, 6s'[1/2]°0 upper levels and 4s[3/2]°2 lower level involved in the two-photon transitions around 13988cm $^{-1}$. Similarly, the 4p'[1/2] 1 serves as near resonant intermediate state for two-photon transitions around 14353 cm $^{-1}$. have also made parallel observations in LOG spectrum of neon. The effects of linear and circular polarization on these two-photon LOG signals. The one-photon lines located between the two pairs of two photon transition may be used as calibration marks for the change in relative intensities of the two-photon lines. The two photon intensity ratioΩ (circular/linear) is found to be 1.5, 1.1, 1.3 and 0.9 for transitions to 5d[1/2]°1, 5d[1/2]°0, 6s'[1/2]°1 and 6s'[1/2]°0 upper levels respectively from the metastable 4s[3/2]°2 level. This observation does not follow the polarization behaviour found for other two-photon transitions with unequal J for upper and lower states (see preceding paragraph). The near resonance of the intermediate states and the important role of collision induced ionization in the generation of LOG signals may be responsible for unusual polarization characteristics of these transitions.

Table 1: Intensity Ratio (Ω) Circular to Linear Polarized Radiation of the Two-Photon Transitions.

Transition frequency(cm^{-1})	Assignment		Experimental (Ω)	Calculated(Ω)
	Upper state	Lower state		
13976.6	6s'[1/2]°0	4s[3/2]°2	(0.9 ± 0.1)	1.5
14008.8	6s'[1/2] ° 1	4s[3/2]°2	(1.3 ± 0. 1)	1.5
14079.2	5d'[5/2]°3	4s'[1/2]° 1	(2.0 ± 0.1)	1.5
14091.6	5d[1/2] ° 1	4s[3/2] ° 1	(0.7 ± 0.2)	1.0
14168.4	5d[3/2]°2	4s[3/2] ° 1	(2.1 ± 0.2)	1.5
14204.5	5d[7/2]°3	4s[3/2] ° 1	(1.9 ± 0.2)	1.5
14266.5	5d[5/2]°2	4s[3/2] ° 1	(2.1 ± 0. 1)	1.5
14290.5	5d' [5/2]°3	4s[3/2] ° 1	(2.0 ± 0. 1)	1.5
14324.9	5d[1/2]°0	4s[3/2] ° 2	(1.1 ± 0. 1)	1.5

14365.0	7s[3/2] ° 1	4s[3/2] ° 1	(0.9 ± 0.2)	1.0
14382.0	5d[3/2] °1	4s[3/2] ° 1	(0.8 ± 0.2)	1.0
14393.7	5d[1/2]° 1	4s[3/2] ° 2	(1.5 ± 0.1)	1.5
14410.0	5d'[3/2]°2	4s'[1/2]°0	(2.0 ± 0.2)	1.5
14445.9	5d[7/2]°4	4s[3/2] ° 2	(2.1 ± 0.2)	1.5
14471.7	5d[3/2]°2	4s[3/2] ° 2	(0.7 ± 0.2)	0.6
14475.7	5d'[5/2]°2	4s'[1/2]°0	(1.9 ± 0.2)	1.5
14508.7	5d[7/2]°3	4s[3/2] ° 2	(2.0 ± 0.2)	1.5
14592.8	5d[5/2]°3	4s[3/2] ° 2	(2.0 ± 0.2)	1.5
14648.7	7s[3/2]°2	4s[3/2] ° 2	(0.7 ± 0.2)	0.6

The lowest excited levels in Ar (electronic configuration 3p54s) in the order of increasing energy are: 4s[3/2]°2, 4s[3/2]°1, 4s' [1/2]°0 and 4s' [1/2]°1 (See Fig. 12) of which the first three are primarily 3p in character and the last one is 1P in the L-S coupling scheme. 4s[3/2]°2 and 4s' [1/2]°0 are truly metastable whereas 4s[3/2]°1 is not quite so due to slight triplet-singlet mixing and 4s' [1/2] °1 has a dipole-allowed transition to the ground state [49]. The next set of excited energy levels arise from the 3p54p configuration and decay primarily to the 4s and 4s' levels With radiative life time in the range of 10-20ns. Temporal profile of the LOG voltage signal resulting from two excited states is given by [22]:

$$\Delta V = -V_0(n_1 - n_2)\left[a_2\, e^{\frac{-t}{T_2}} - a_1\, e^{\frac{-t}{T_1}}\right] \qquad (25)$$

Where a_2,a_1 (a_2>a_1) represent the electron-impact ionization coefficients T_2,$T_1$the relaxation times and n_2,$n_1$the atomic populations of the upper and lower energy levels respectively. V_0 is a constant for a particular transition and depends on its optical absorption cross section.

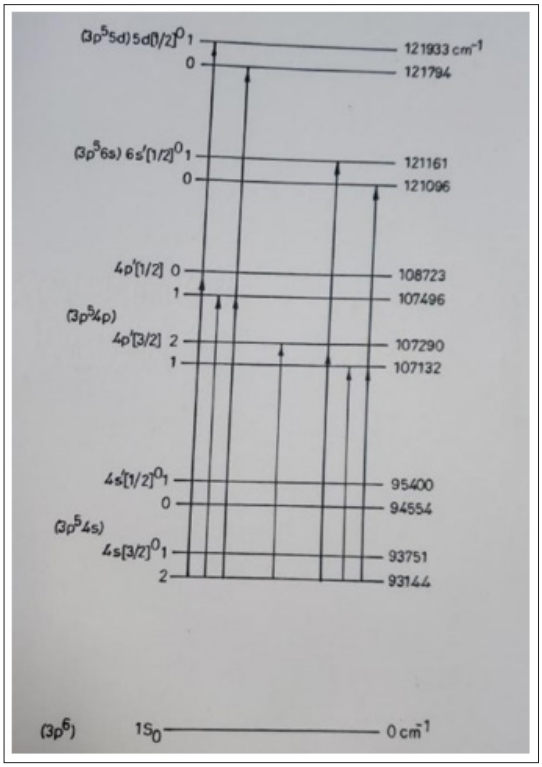

Figure 11: Partial Energy Level Diagram of Ar to Illustrate Near Resonant two Photon Transition are Indicated by Heavy Arrows and one Photon Transition by Light Arrows.

In the temporal profile of the LOG signals immediately following the laser excitation pulse (t = 0), the voltage is negative due to the dominance of the first term within the square brackets of Equation (15). This behavior is observed for all the transitions depicted in Figure 11(b). For the optogalvanic transitions with the 4s[3/2] °2 state as the lower state and the 4p'[3/2] 2, 4p'[1/2] 1 states as the upper states, the signals are positive for long delay times (Figure 10(a)) but negative for short delay times (Figure 10(b)) after the excitation laser pulse. The composite negative and positive LOG signals arise because of the condition T_2<T_1, such that the first term in Equation (17) dominates at short delay times, while the second term becomes more dominant for longer delays. In the case of two-photon transitions,

the LOG signal remains negative even for longer delays after the excitation pulse. This indicates that the relaxation time of the upper state in these transitions is comparable to that of the lower state, in accordance with Equation (15).

The observed ratio of two-photon intensities with circular and linear polarization can generally be classified into two categories. For transitions where the upper and lower states have equal (J)-values, the polarization ratio (Ω) is approximately 0.7, while for transitions with unequal (J)-values, the ratio is close to 2 (see Table 1). However, four of the strongest two-photon lines deviate from this expected polarization behavior, as discussed in the following paragraph. Greenberg et al. conducted a detailed analysis of LOG intensity, considering both the scalar and quadrupolar components of the two-photon transition tensor for the Doppler-free two-photon spectrum of neon [37,38]. Their analysis concluded that the experimental polarization characteristics did not align with theoretical predictions unless accurate wave functions for the initial, final, and intermediate states were used. The observed experimental values of the polarization ratio (Ω) were compared with those predicted by theoretical studies [21,22].

The exceptionally large intensities observed for two pairs of two-photon transitions, as shown in Figures 10(b) and 10(c), can be attributed to the near resonance of the intermediate states (Figure 12). Specifically, the 4p'[3/2] °1 level is situated nearly midway between the 6s'[1/2] °1, 6s'[1/2] °0 upper levels and the 4s[3/2] °2 lower level involved in the two-photon transition around 13,988 cm^{-1}. Similarly, the 4p'[1/2] °1 level serves as the near-resonant intermediate state for two-photon transitions around 14,353 cm^{-1} (Figure 11). Biraben et al. [38] made similar observations in the LOG spectrum of neon, particularly regarding the effects of linear and circular polarization on these two-photon LOG signals. The one-photon lines located between the two pairs of two-photon transitions may be utilized as calibration markers to monitor the changes in the relative intensities of the two-photon lines.

The two-photon intensity ratios Ω (circular/linear polarization) were found to be 1.5, 1.1, 1.3, and 0.9 for the transitions from the metastable 4s[3/2] °2 level to the upper levels 5d[1/2] °1, 5d[1/2] °0, 6s[1/2] °1, and 6s[1/2] °0, respectively. These observations do not conform to the polarization behavior typically observed for other two-photon transitions with unequal JJ-values for the upper and lower states (as seen in the preceding graph). The near-resonance of the intermediate states, coupled with the significant role of collision-induced ionization in the generation of optogalvanic signals, may account for the unusual polarization characteristics of these transitions [38].

In the Dye region III, the relative intensities of two photon transition were also determined for circularly polarized light and the ratioΩ of circular to linear polarization intensities is included in the last column of Table 1. The linear and circular polarization spectrum in the frequency range 15580 to 16200 cm-1 of dye region III is given. The intensity ratio of two photon for transition with equal of J for the upper and lower state is found to be 0.98 and for those with unequal J nearly equal to 1.4. these number however less reliable in comparison to intensity ratios for transition of dye region II.

The LOG spectrum of argon (Ar) has been previously studied by Nestor in the wavelength range of 695-795 nm, by M.C. Su et al. in the wavelength range of 555-575 nm, and by Reddy et al. in the wavelength range of 415-670 nm [25-27, 29]. These studies focused solely on one-photon transitions in Ar discharge. In the present work, we report the first observation of two-photon transitions in an Ar discharge, alongside the assignment of several new one-photon transitions in the wavelength range of 605-740 nm. To facilitate comparison of our one-photon optogalvanic transitions with previous studies, the transition frequencies from M.C. Su et al. and Reddy et al. are provided in Table 2, along with the standard values from Moore's table [26,28,29]. The transition frequencies obtained in this study are also included in Table 2.

1. It can be seen that optogalvanic one photon transitions in the frequency range 13523 cm-1 to 14956 cm-1 have been observed for the first time in the present work.
2. The observed transition frequencies of the present work agree with the optogalvanic transition frequencies of Reddy et al. with an uncertainty not exceeding ±1 cm-1 except in those cases where errors in the assignment exist in the earlier work [29].

a. The transitions frequency of 17570.1cm-1 (5689.91Å) assigned 6d^' [3⁄2]^° 2→4p^' [3⁄2]1 in reference corresponds to a transition frequency of 17934.8 cm-1 according to the energy level tables of Moore [28]. The transition frequency 17570.7cm-1 (5689 Å) assigned as 5d^' [3⁄2]^° 1→4p[3⁄2]2 in reference corresponds to a transition frequency of 17577.9cm-1 according to the energy level table of Moore [3,39]. Thus the assignments of reference should be 6d^' [3⁄2]^° 2→4p^' [1⁄2]1 at frequency 17570.1 cm-1 which agrees with standard tables[3,39].
b. The transition frequency of 16496.2cm-1(6060.3 Å) assigned as 4d^' [5⁄2]^° 2→4p[1⁄2]1 in reference corresponds to a transition frequency of 16516.9cm-1 according to the energy levels table of Moore [28]. In the present work the transition frequency at 16498.5 cm-1 has been assigned as 4d^' [3⁄2]^° 2→4p[1⁄2]1 and the deviation of about 2cm-1 may be due to error in measurements.
c. The transition frequency of 16437.1cm-1 (6082.1Å) is assigned as 6d^' [3⁄2]^° 1→4p^' [1⁄2]1 in reference but the value of upper energy level is not given in reference [28,29]. In the present work an optogalvanic line at 16439.1cm-1 has been assigned as 8s[3⁄2]^° 1→4p^' [1⁄2]1 with a transition frequency of 16439.5cm-1 according to the standard table by [28]. Thus the assignment of reference by need to be corrected and again there is a deviation of about 2cm-1 in the measurement of this line [27,29].
d. The transition frequency of 15290.7cm-1 (6538.1 Å) assigned as 4d^' [3⁄2]^° 2→4p[5⁄2]3 in reference corresponds to a transition frequency of 15138.1cm-1 according to the energy levels tables of Moore [28,29]. In the present work the transition frequency at 15290.7cm-1 has been assigned as 4d^' [5⁄2]^° 3→4p[5⁄2]3 in agreement with the value from Moore [28].
e. The transition frequency of 15156.9 cm-1 (6571.4 Å) is assigned as 6d[3⁄2]^° 1→4p^' [1⁄2]0 in reference but the value of upper energy level is not given in reference [28, 29]. in the present work an optogalvanic line at 15155.7cm-1 has been assigned as 4d^' [5⁄2]^° 2→4p[5⁄2]3 with a transition frequency 15156.2cm-1 according to the standard table [3].
f. The transition frequency of 15002.3cm-1(6663.8 Å) assigned as4d^' [3⁄2]^° 2→4p[5⁄2]2 in reference corresponds to a transition frequency of 14983.6cm-1 according to the energy level tables of Moore [28,29]. In the present work the transition frequency at 15002.0 cm-1 has been assigned as 4d^' [5⁄2]^° 2→4p[5⁄2]2 in agreement with the value from Moore [28].

Some of the optogalvanic transitions in the frequency range 13523cm-1 to 14956cm-1 of the present work were also reported by Nestor as shown in table-3 Nestor however characterized this transition only on the basis of the positive or negative voltage signal and did not mention their assignments [25]. These assignments are already given in Table 2.

Table 2: Relative Intensity of Tunable Dye Laser Wavelength Regions and Transition States

Frequency(cm^{-1})	Relative Intensity	Upper state	Lower state	Transition type (Ω)
13523.2	03	6s [3/2]°1	4p [3/2]2	OP
13539.9	18	4p' [3/2]2	4s [3/2]o1	OP
		7s[3/2]°1	4s' [1/2]o1	TP
13561.4	10	4d [7/2]°4	4p [5/2]3	OP
13595.3	12	4d [7/2] °3	4p(5/2]2	OP
13610.5	04	4d [3/2] °1	4p [3/2]2	OP
13664.8	07	6s' [1/2]°1	4p' [1/2]1	OP
13673.2	04	6s[3/2]°1	4p [3/2]1	OP
13705.4	14	6s' [1/2]°1	4s [3/2]°1	TP
13722.1	05	4d' [3/2]°1	4p' [3/2]2	OP
13745.8	35	4p' [1/2]1	4s[3/2]°1	OP
13749.9	17	4d [7/2]°3	4p [5/2]3	OP
13757.1	03	7s [3/2]°1	4p' [1/2]0	OP
13760.5	05	4d [3/2]°1	4p [3/2]1	OP
13804.9	06	4d' [5/2]°3	4s [3/2]°2	TP
13827.5	09	4d [5/2]°2	4p [5/2]2	OP
13872.0	17(b)	6s' [1/2]°1	4p' [3/2]2	OP
13880.0	05	4d' [3/2] °1	4p' [3/2]1	OP
13930.0	05(b)	-	-	-
13944.4	05	7s[3/2]°2	4s' [1/2]°0	TP
13948.3	07	4d [5/2]°3	4p[5/2]2	OP
13976.6	70	6s' (1/2]°o	4s[3/2]°2	TP(0.9±0.1)
13988.3	60	4p' [3/2] 1	4s[3/2]°2	OP
14008.8	80	6s' (1/2]°1	4s[3/2]°2	TP(1.3±0. 1)
14079.2	06	5d' [5/2]°3	4s' [1/2]°1	TP(2.0±0. 1)
14091.6	11	5d [1/2]°1	4s[3/2]°1	TP(0.7±0. 2)
14104.3	04	4d [5/2]°3	4p [5/2]3	OP
14128.2	06	6d [7/2]°4	4s' [1/2]°1	TP(1.9±0.2)
14145.9	100	4p' [3/2]2	4s [3/2]°2	OP
14168.4	07	5d [3/2]°2	4s[3/2]°1	TP(2.1±0.2)
14204.5	06	5d [7/2]°3	4s[3/2]°1	TP(1.9±0. 2)
14222.3	03	4d [5/2]°3	4p [5/2]3	OP
14231.8	02	4d [3/2]°1	4p[5/2]2	OP
14266.5	04	5d [5/2]°2	4s [3/2]°1	TP(2.1±0.1)
14290.5	02	5d' [5/2]°3	4s[3/2]°1	TP(2.0±0. 1)
14297.8	02	6s [3/2]°1	4p [5/2]3	OP
14324.9	100	5d [1/2]°o	4s [3/2]°2	TP(1.1±0. 1)
14352.7	65	4p [1/2] 1	4s [3/2] °2	OP
14365.0	15	7s[3/2]°1	4s[3/2]°1	TP(0.9±0.2)
14382.0	06	5d [3/2]°1	4s[3/2]°1	TP(0.8±0.2)
14393.7	65	5d [1/2]°1	4s [3/2]2	TP(1.5±0.1)
14410.0	07	5d' [3/2]°2	4s' [3/2]°0	TP(2.0±0.2)
14445.9	13	5d [7/2] °4	4s [3/2]°2	TP(2.1±0.2)
14471.7	20	5d [3/2]°2	4s [3/2]°2	TP(0.7±0.2)

14475.7	05	5d' [5/2)°2	4s' [3/2]°o	TP(1.9±0.2)
14508.7	03	5d [7/2]°3	4s[3/2] °2	TP (2.0±0.2)
14515.3			(unassigned)	
14550.5	03	4d [1/2]°1	4p[1/2] 1	OP
14590.8	15	5d [3/2]°2	4p' [1/2] 1	OP
14592.8	04	5d [5/2]°3	4s[3/2]°2	TP (2.0±0.2)
14648.7	09	7s[3/2]°2	4s [3/2]°2	TP(0.7±0.2)
14785.7	10	5d [5/2]S°2	4p' [1/2] 1	OP
14803.1			(unassigned)	
14924.5	25	4d' [3/2]°1	4p[3/2]1	OP
		69' [1/2]°1	4p[3/2]2	OP
14944.5	08	7s [3/2]°2	4p' [1/2]1	OP
14956.2	20	5d [3/2]°2	4p' [3/2] 1	OP
14972.5	40	4p' [1/2]0	4s[3/2]°1	OP
14983.5	18	4d' [3/2]°2	4p [5/2]2	OP
		7s[3/2]°1	4p' [1/2] 1	OP
15002.0	35	4d' [5/2]°2	4p[5/2]2	OP
15010.1	04	6s' [1/2]°0	4p [3/2] 1	OP
15018.1	08	5d [3/2]°1	4p' [1/2] 1	OP
S15039.7	10 (b)	5d [5/2]°3	4p' [3/2]2	OP
15065.5	09	7s' [1/2]°1	4s [3/2]°1	TP
15074.7	09	6s' [1/2]°1	4p [3/2]1	OP
15093.2	08	8s[3/2]°1	4s[3/2]°1	TP
15114.5	30	5d' [3/2]°2	4s[3/2]°2	TP
15136.2	70	4d' [5/2]°3	4p [5/2]2	OP
15137.8	75	4d' [3/2]°2	4p [5/2]3	OP
15150.2	28	5d[5/2]°2	4p' [3/2] 1	OP
15155.7	60	4d' [5/2]2	4p [5/2]3	OP
15161.2	06	6d [1/2)°1	4s[3/2]°2	TP
15181.8	06	6d [1/2]°0	4s [3/2]°2	TP
15190.1	06	7s [3/2]°1	4p' [3/2]2	OP
15213.7	09	8s [3/2]°1	4p [1/2]0	OP
15224.8	06	5d [3/2]°1	4p' [3/2]2	OP
15254.0	20	6d [7/2]°4	4s[3/2]°2	TP
15273.6	07	10d [5/2]°2	S4s' [1/2]°1	TP
15279.2	07	6d' [5/2]°2	4s' [1/2]°0	TP
15290.7	90	4d' [5/2]°3	4p [5/2]3	OP
15308.1	07	7s[3/2]°2	4p' [3/2] 1	OP
15342.2	25	4d [5/2]°2	4p [1/2]1	OP
15347.0	12	7s[3/2]°1	4p' [3/2] 1	OP
15379.1	14	8s [3/2]°2	4s[3/2]°2	TP
15382.5	12	5d [3/2]°1	4p' [3/2]1	OP
15394.4	28	4d' [3/2]°1	4p [5/2]2	OP
15426.1	05	7s[3/2]°1	4p[1/2]0	OP
15449.2	03	7d [7/2]°3	4s [3/2]°1	TP
15460.8	08	5d [3/2]°1	4p [1/2]0	OP
15491.7	03(b)		unassigned	
15515.9	03	13d [5/2]°3	4s[3/2]°1	TP
15544.3	25	6s' [1/2]°1	4p [5/2]2	OP

15580.9	100	6s[3/2]°2	4p[1/2] 1	OP
15624.8	02 (b)		unassigned	
15641.7	03(b)		unassigned	
15657.3	75	6s[3/2]°1	4p [1/2]1	OP
15695.1	50	5d [1/2]°1	4p [3/2]2	OP
15706.4	30	5d [1/2]°0	4p[3/2]1	OP
15729.8	08	7d [3/2]°2	4s[3/2]°2	TP
15732.8	14	7d [7/2]°4	4s[3/2]°2	TP(1.42± 0.1)
15744.8	35	4d [3/2]°1	4s[1/2]1	OP
15785.1	03	7d [5/2]°3	4s[3/2]°1	TP(1.40± 0.2)
15790.2	03	10s [3/2]°1	4s[3/2]°1	TP(0.98±S 0.1)
15813.6	13	9s [3/2]°2	4s[3/2]°1	TP
15832.6	07	7d [1/2]°1	4p'[1/2]0	OP
15845.6	50	5d [1/2]°1	4p[3/2]1	OP
15849.8	70	5d [3/2]°2	4p[3/2]2	OP
15877.0	25	5d' [3/2]°2	4p'[1/2]1	OP
15922.6	40	5d [7/2]°3	4p[3/2]2	OP
15961.7	04	6d' [7/2]°2s	4s[3/2]°2	OP
15972.1	15	6d [1/2]°1	4p' [1/2] 1	OP
16000.7	25	5d [3/2]°2	4p [3/2] 1	OP
16009.9	12	8d [1/2]°0	4s[3/2]°2	TP(1.40± 0.1)
16013.0	12	6d [1/2]°0	4p'[1/2]1	OP
16037.7	06	8d [7/2]°4	4s[3/2]°2	TP(1.42± 0.1)
16045.4	35	5d [5/2]°2	4p[3/2]2	OP
16083.5	60	5d' [3/2]°2	4p'[3/2]2	OP
16092.9	75	5d [5/2]°3	4p[3/2]2	OP
		10s [3/2]°2	4s[3/2]°2	TP(1.16 ±0.1)
16127.2	03		unassigned	
16165.5	25(b)		unassigned	
16178.8	13	6d [1/2]°1	4p' [3/2] 2	OP
16195.5	40	5d [5/2]°2	4p[3/2] 1	OP
16202.7	55	7s[3/2]°2	4p[3/2]2	OP
		11d [7/2]°3	4s[3/2]°1	TPP (1.9±0.2)
16216.4	40	5d' [5/2]°2	4p' [3/2] 2	OP
16242.4	50	7s[3/2]°1	4p [3/2]2	OP
16267.8	30	5d' [5/2]°3	4p' [3/2] 2	OP
16276.7	17	5d [3/2]°1	4p [3/2]2	OP
16312.3	14	6d [3/2]°2	4p' [1/2] 1	OP
16315.5	28	5d [1/2]°1	4p [5/2]2	OP
16318.7	14	5d' [3/2]°1	4p' [1/2]1	OP
16329.9	13	6d [5/2]°2	4p' [1/2] 1	OP
16336.3	14	6d [1/2] °1	4p' [3/2] 1	OP
16353.1	13	7s[3/2]°2	4p [3/2]1	OP
16376.3	50	6d[1/2]°0	4p' [3/2]1	OP
16386.0	45	7s' [1/2]°1	4p' [1/2] 1	OP
16391.2	40	7s[3/2]°1	4p[3/2]1	OP
16406.2	05	8s [3/2]°2	4p' [1/2]1	OP
16413.3	30	6d [1/2]°1	4p[1/2]0	OP
16426.2	10	5d [3/2]°1	4p [3/2]1	OP

16439.1	10	8s[3/2]°1	4p' [1/2]1	OP
16453.0	15 (b)		unassigned	OP
16483.9	12	6d [7/2]°3	4p' [3/2]2	OP
16498.5	25	4d' [3/2]°2	4p[1/2]1	OP
16516.0	18	4d' [5/2]°2	4p[1/2]1	OP

Table 3: Transition Frequencies of Present work and with Earlier References

Transition frequency from Ref[7]	Transition frequency from Ref[11]	Transition frequency from Ref[9]
17984.8	17985.1	17984.3
17940.4	17940.3	17940.1
17910.3	17910.4	17910.1
17888.2	17888.6	17888.2
17860.2	17861.4	17860.3
17856.9	17857.6	17856.9
17850.8	17849.6	17850.7
17835.4	17334.9	17835.4
17830.7	17830.8	17830.8
17794.9	17794.9	17795.0
17785.8	17786.4	17786.3
17776.7	17776.0	17776.4
17739.4	17740.0	17739.8
17698.4	17698.2	17698.5
17692.0	17692.0	17692.5
17665.6	17665.4	17665.6
17594.9	17595.4	17594.9
17589.2	17589,7	17589.2
17570.1	17570.7	17570.1
17536.3	17536.8	17536.4
17418.2	17418.3	17418.2
16977.2	-	16977.6
16909.7	-	16909.4
--	16516.0	16516.8
16496.2	16498.8	16498.3
-	16483.9	16484.2
16449.8	16453.0	Unassigned
16437.1	16439.1	16439.5
16424.9	16426.2	16426.6
	16413.3	16413.7
16406.9	16406.2	16406.7
-	16391.2	16392.0
-	16386.0	16385.4
-	16376.3	16377.2
-	16353.1	16352.8
-	16336.3	16336.3
16329,2	16329.9	16330.1
-	16318.7	16319.0
16316.1	16315.5	16315.8
16311.8	16312.3	16312.0
16276.5	16276.7	16277.1
16267.5	16267.8	16268.0
16242.1	16242.3	16242.3
16216.9	16216.4	16216.6
16202.1	16202.7	16202.6
16194.1	16195.5	16194.8
-	16178.8	16178.3
-	16166.5	Unassigned
-	16127 .2	Unassigned
16093.4	16092.9	16092.1
16083.5	16083.5	16083.3
	16045. 4	16044.s7
16012.2	16013.0	16012.5
15999.4	16000.9	15999.6
15972.5	15972.1	15972. 4
15922.4	15922.6	15922.6
15877. 4	15877.0	15877.2
15850.1	15849.8	15849.7
15846.4	15845.6	15845.6
-	15832.6	15832.3
-	15744.8	15745.2
-	15706.4	15706.8
15695.9	15696.1	15696.0
15658.1	15657.3	15658.1
-	15641.7	unassigned
-	15624.8	unassigned
15581.0	15580.9	15581.2
-	15544.0	15544.0
-	15491.7	unassigned
15459.8	15460. 8	15460.0
-	15426.1	15425.4
-	15394.4	15394.6
-	15382.5	15382.6
15347 .7	15347.7	15347.7
-	15342.2	15342.7
-	15308. 1	15308.3
15290.7	15290. 4	15291. 0
-	15224.8	15224.6
-	15213.7	15213.4
-	15190.1	15189.8
15156.9	15155.7	15156.2
-	15150.2	15150.3

-	15137.8	15138. 1
-	15136.2	15136.2
-	15074.7	15074.2
-	15039.7	15040.0
-	15018.1	15018.0
-	15010.1	15009.7
15002.3	15002.0	15001.7
-	14983.5	14983.6
14971.9	14972.5	14972.0
-	14955.2	14956.4
-	14944.5	14944.2
-	14924.5	14925.2
-	14803.1	Unassigned
-	14785.7	14786.0
-	14590.8	14590.2
-	14550.5	14550.2
-	14515.3	Unassigned
14352.0	14352.7	14353.0
-	14297.8	14298.0
-	14231.8	14232.0
-	14222.3	14222.1
14146.0	14145.9	14146.1
-	14104.3	14104.3
13988.0	13988.3	14988.1
-	13948.3	14948.7
-	13930.0	Unassigned
-	13880.0	13880.1
-	13872.0	13871.6
-	13827.5	13827 .5
-	13760.5	13760.8
-	13757.1	13757.7
-	13749.9	13750.1
13745.0	13745.8	13745.8
-	13722.1	13722.2
-	13673.2	13673.4
-	13664.8	13665.1
-	13610.5	13610.2
-	13595.3	13594.9
-	13561.4	13560.9
13539.0	13539.9	13540.1
-	13523.2	13523.5

A method for electric field measurement based on the laser spectroscopy of argon atoms was developed and calibrated by Jung-Bae Kim et al. [40]. The measurements were performed using LOG spectroscopy, with several different transitions in argon examined. It was found that the 4s - 7f and 4s - 8f transitions were particularly well-suited for measurements in the sheath region of glow discharges. The lower detection limit for electric field measurements was estimated to be 500 V/cm. A minimum pressure of approximately 100 mTorr was required to detect LOG signals, while around 1 Torr was necessary for the fluorescence signals to be observable.

Glow discharge plasmas have a wide range of applications across various industries, including manufacturing and lighting. For instance, discharge plasmas are extensively utilized in the microelectronics sector for processes such as etching, deposition, and other plasma-based surface treatments. The optimization of plasma conditions is often performed empirically by modifying discharge parameters, such as electrode shape, gas type and pressure, and applied voltage. However, to advance plasma applications, it is essential to develop a more systematic understanding of the fundamental discharge mechanisms.

The properties of plasmas used in deposition, etching, and other industrial applications are influenced by numerous factors, particularly the energy distribution functions of charged particles and the flux of these particles. These factors are, in turn, determined by the shape and magnitude of the electric field throughout the discharge, especially the sheath electric fields present at the interface between the plasma and the surrounding surfaces. A comprehensive understanding of charged particle transport within the sheath is crucial for enhancing the control and optimization of industrial plasma systems.

Consequently, significant efforts have been devoted to studying the sheath region and its associated electric fields. Techniques such as electric probes and emission spectroscopy are commonly employed to measure electric field distributions. While these methods are relatively simple, they are not without drawbacks. Electric probes can perturb the plasma, and there is often ambiguity in interpreting the resulting data. Emission spectroscopy, on the other hand, lacks spatial resolution and provides limited information. Laser diagnostic methods offer clear advantages, as they provide similar information without disrupting the plasma and, in principle, offer high spatial and temporal resolution.

Experimentally, the plasma was generated by applying a direct current (dc) voltage across two planar stainless steel electrodes, each with a diameter of 40 mm and separated by 15 mm. A constant dc current of 20 mA was maintained to sustain the plasma. The electrodes were positioned at the center of a cylindrical stainless steel vacuum chamber with a diameter of 250 mm and a height of 320 mm.

The laser source employed in the experiment was a tunable dye laser, which was pumped by a xenon chloride excimer laser. The dye laser was operated at a specific wavelength (in nm), and its output was frequency-doubled to generate the required radiation at another wavelength (in nm) for the experiment. The dye laser emitted pulses with a duration of 25 ns and a spectral width of 0.2 cm^{-1}. The laser beam was directed through the plasma parallel to the electrode surfaces. A cylindrical lens was used to focus the beam in one dimension, resulting in an elongated cross-section of the beam within the plasma, with a beam width of 0.2 mm in the direction perpendicular to the electrode surface.

The absolute wavelength of the dye laser was monitored by directing its fundamental output into an argon hollow cathode lamp. Simultaneously, the LOG spectrum from the plasma was recorded alongside the spectrum of known argon lines, allowing for precise wavelength calibration.

Two-photon LOG spectra of argon in the visible region is also studied by N K Piracha et al. using an excimer-pumped dye laser in conjunction with an argon discharge cell [41]. The experimental method enables us to record a pure two-photon spectrum in a region which is full of one-photon transitions. Eleven Rydberg series originating from the 3p5(2P3/2),4s[3/2]2 and 3p5(2P1/2), 4s0 [1/2]0 metastable levels have been observed. It is noticed that the strongest signals are for the 3p5nd[7/2]4 series excited from the 3p54s[3/2]2 metastable level. Inter channel interaction among the J = 3 and J = 2 have been parametrized using three- and five-channel quantum defect theory respectively.

The discharge was operated at a voltage of 220 V, with a ballast resistor of 70 kΩ, and the optogalvanic voltage was monitored through a coupling capacitor of 0.1 μF. The laser was focused into the discharge cell using an 80 mm focal-length lens. The discharge was initially sustained by an electron-impact, two-step ionization process, as described by Barbieri et al. [43].

i.e.

$$Ar(^1S_0) + e^- \rightarrow Ar(3p^5\ 4s) + e^-$$

$$Ar(3p^5 4s) + e^- \rightarrow Ar^+ + 2e^-.$$

Thereby generating a considerable amount of argon atoms in the 3p54s metastable state multiplets. The laser shifts the metastable 3p54s population to Rydberg levels whose lifetime vary with $(n - \mu)3$ where μ is the quantum defect. The increased Rydberg state population then contributes in enhancing the ionization process. The discharge impedance decreases and a negative voltage signal pulse results. This can be explained by the rate equation model presented by Erez et al. For the wavelength calibration of the experimental data, a commercial hollow cathode lamp filled with argon was simultaneously irradiated with the same laser (figure 13) [16]. The signals from the commercial hollow cathode lamp and the discharge cell were processed by two SRS boxcar averagers (SR 250) and recorded on a dual channel chart recorder. The signals obtained from the hollow cathode lamp, using the assignments of Striganov and Sventitskii (1968), served as the frequency markers for the measurement of the argon spectrum obtained from the discharge cell.

Argon (Z=18) has 26 known isotopes, from 29Ar to 54Ar of which three are stable (36Ar, 38Ar, and 40Ar). Isotope 40Ar, which makes up 99.6% of natural argon on the Earth, does not have a hyperfine structure (nuclear spin quantum number I = 0).

LOG spectroscopy is based on the detection of small changes in the plasma impedance caused by resonant absorption of monochromatic light of a tuneable laser [43]. Hollow cathode discharges have proven to be particularly suitable for such studies. The experimental investigation of electronic levels near the ionization threshold presents challenges, as classical fluorescence detection methods are inefficient for detecting highly excited levels. This issue can be addressed using LOG spectroscopy. In this technique, the discharge excites the atoms to intermediate energy levels, and then a modulated laser beam transfers the atoms from these intermediate levels to the levels of interest, thereby modulating the discharge conductivity.

Argon atomic levels were excited using a continuous discharge, with typical discharge currents ranging from 65 to 90 mA and voltages between 500 and 700 V. The discharge excites the atoms to intermediate energy levels, after which the modulated laser beam further excites the atoms to higher levels. The laser light was produced by a continuous-wave (cw) ring dye laser, which was pumped by a 532 nm laser and operated with the dye Kiton Red 620.

The Zeeman effect measurements were conducted in magnetic fields generated by two distinct sets of permanent neodymium magnets, producing fields of approximately 700 G and 1200 G in the observation region. To obtain precise magnetic field measurements, the Zeeman effect was observed for two intense argon spectral lines, specifically at 605.2723 nm and 605.9372 nm. The calibration data for the magnetic fields were obtained from the NIST database.

In the present study, we investigated the Zeeman structure of 10 argon spectral lines with wavelengths ranging from 598.7 to 610.6 nm. The measurements were conducted for two mutually perpendicular polarization directions of the exciting laser beam to obtain the π and σ patterns. A half-wave plate and a Glan prism polarizer were used for polarization control. Due to the non-distinct nature of the σ polarization spectra for all the examined lines consisting only of a single broad peak we refrained from performing a quantitative analysis of these σ spectra.

For the computer analysis of the recorded Zeeman structures, we utilized software developed within our research group. We assumed that the observed optogalvanic signal contours could be described by a modified Lorentzian profile. This program has been thoroughly tested in previous studies conducted by our group. The input data for the program include the quantum numbers J of the upper and lower states, the magnetic field strength, and the direction of the observed polarization. The output data comprise the Lande factors for the upper and lower states of the transition, as well as the line shape parameters. In the present study, we focused solely on determining the Lande factor for the upper state, as the spectral structure was not sufficiently distinctive to allow for the determination of both Lande factors as free parameters. The observed line structures consisted of two broad peaks, and an unambiguous, precise analysis would not be feasible without knowledge of both gJ values for the upper and lower states.

As an example, Figs. 12 and 13 present the Zeeman structures of two argon lines, 604.3223 nm and 611.9656 nm, alongside the corresponding computer-generated profiles. The permanent magnets were placed in a container with liquid nitrogen near the observation region, which resulted in slight variations in the magnetic field values for each measurement series. The magnetic field strength was determined each time after altering the polarization of the laser light or adjusting the laser beam passing through the hollow cathode lamp. Additionally, small positional changes in the magnets could occur when liquid nitrogen was replenished, necessitating a recalibration of the magnetic field before each new series of measurements.

The atomic lines selected for our study were chosen such that, for each line, one of the required gJ values for analyzing the Zeeman spectrum was known. We assumed that the gJ values for the lower-lying states had been precisely determined and verified. The NIST database was utilized for this purpose. In the computer analysis, the gJ values for the lower states were fixed, while the only free parameters were the gJ value for the upper state and

two line shape parameters. Each reported value represents the arithmetic mean of approximately ten measurements conducted under different experimental conditions for two distinct magnetic field values. Statistical errors, indicated in brackets, were corrected using Student's t-distribution coefficients.

For the three levels at 122160.1502, 123882.203, and 123935.870 cm^{-1}, we were able to determine the Lande factors by analyzing the Zeeman structures of two lines. The results obtained from examining these different lines were consistent, as evidenced by the $\chi 2$ test values, which were all less than 1.

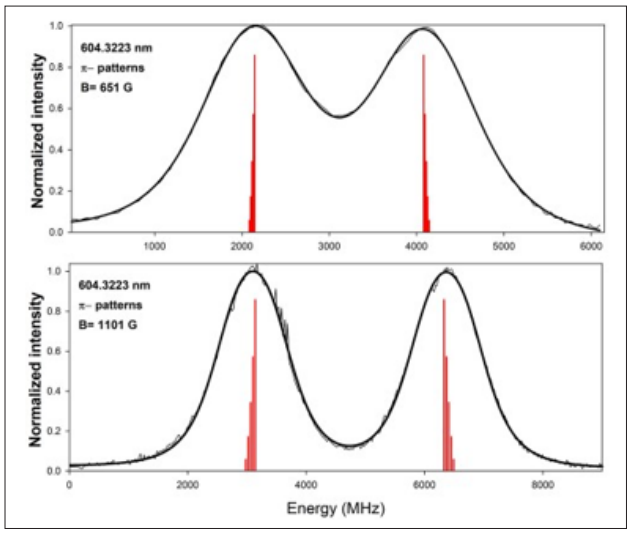

Figure 12: Zeeman Structure Recorded using LOG Spectroscopy.

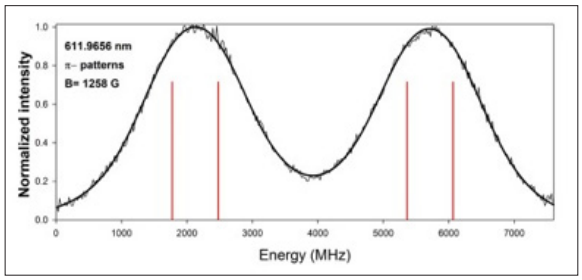

Figure 13: Zeeman Structure Recorded using LOG Spectroscopy.

The LOG spectroscopy employed in our measurements provided new spectroscopic data and contributed to the verification of previously reported experimental results. We determined the experimental Lande gJ factors for levels with odd parity.

Conclusion

A comprehensive analysis of argon's one- and two-photon LOG spectra in the 605–740 nm wavelength range has been conducted. While the two-photon transition profiles exclusively exhibit a negative voltage signal, one-photon transitions display a composite temporal profile that includes both positive and negative voltage signals. Experiments involving linear and circular polarization have been used to differentiate between various types of two-photon transitions. Notably, a near-resonant observation has been achieved where actual energy levels coincide with intermediate levels in the two-photon transitions. This results in anomalous intensity variations in circular and linear polarization, unlike two-photon transitions without actual intermediate levels.

Additionally, polarization dependence has been noted for two-photon transitions. The intensity ratios of argon atoms linear and circular two-photon transitions were measured experimentally and compared to theoretical predictions. The calculated intensities for these polarized two-photon transitions closely align with the experimental results.

Acknowledgments

RCS is highly thankful to Professor S N Thakur, has learned Laser Technologies and Laser Spectroscopic Techniques. RCS is very thankful to Dr V K Saraswat, he always motivated towards R & D as mentor in DRDO. Also, very thankful to Professor K K Sharma, Professor R K Thareja IIT Kanpur, Dr J P Singh ICET Mississippi State University USA, Professor King Lin IAMS Taipei Taiwan fruitful discussion about the LOG spectroscopic technique. Authors are also thankful to use facility of BHU Varanasi carried out experimental work, further extended work is done at LASTEC, DRDO. RCS is also thankful to Dr Chris Webster JPL NASA Pasadena USA for the discussion about the laser spectroscopy and photonics techniques.

No Conflicts Interest

Reference

1. Green RB, Keller RA, Luther GG, Schenck PK, Travis JC (1976) Galvanic detection of optical absorptions in a gas discharge. Applied Physics Letters 29: 727-729.
2. Schenck PK, Smyth KC (1978) Opto-galvanic spectroscopy of atomic neutrals and ions in discharges (A). Journal of the Optical Society of America 68: 626.
3. Suzuki T, Sekiguchi H, Kasuya T (1983) Optogalvanic detection with microwave discharge. Le Journal de Physique Colloques 44: C7-C419.
4. Sharma RC, Das BK, Sharma G, Saraswat VK, Thakur SN (2024) Temporal evolution of opto-galvanic effect in normal glow discharge of argon. Spectroscopy Letters 58: 1-9.
5. Sobolewski ŁM, Kwela J, Windholz L (2021) Optogalvanic spectroscopy of the Zeeman structure of argon energy levels close to the ionization limit. Journal of Quantitative Spectroscopy and Radiative Transfer 272: 107778.
6. Saini VK (2013) Laser-induced optogalvanic signal oscillations in miniature neon glow discharge plasma. Applied Optics 52: 4404-4411.
7. Saini VK, Shrivastava VK, Khare R (2008) Anomalous behavior of optogalvanic signal in a miniature neon discharge lamp. Optics communications 281: 129-134.
8. Shah ML, Mandal PK, Dev V, Suri BM (2012) Study of even-parity autoionization resonances of atomic uranium by three-color optogalvanic spectroscopy. Journal of the Optical Society of America 29: 1625-1630.
9. Haridass C, Major H, Misra P, Han XL (2002) Laser optogalvanic spectroscopy of discharge plasmas in the ultraviolet region. Practical Spectroscopy Series 30: 33-70.
10. Suzuki T, Sekiguchi H, Kasuya T (1983) Optogalvanic detection with microwave discharge. Le Journal de Physique Colloques 44: C7-C419.
11. Stanciulescu C, Bobulescu RC, Surmeian A, Popescu D, Popescu I, et al. (1980) Optical impedance spectroscopy. Applied Physics Letters 37: 888-890.
12. Lawler JE (1980) Experimental and theoretical investigation of the optogalvanic effect in the helium positive column. Physical Review A 22: 1025.
13. Paschen F (1919) Das spektrum des neon. Annalen der Physik

365: 405-453.
14. Colin S Willett (1974) Introduction to gas lasers: Population Inversion Mechanisms, Pergamon Press. New York: 61.
15. Broglia M, Catoni F, Montone A, Zampetti P (1987) Galvanic detection of laser photoionization in hollow-cathode discharges: experimental and theoretical study. Physical Review A 36: 705.
16. Erez G, Lavi S, Miron E (1979) A simplified theory of the optogalvanic effect. IEEE Journal of Quantum Electronics 15: 1328-1332.
17. Wakata S, Hosoya N, Hasegawa N, Nishikino M (2022) Defect detection of concrete in infrastructure based on Rayleigh wave propagation generated by laser-induced plasma shock waves. International Journal of Mechanical Sciences 218: 107039.
18. Marquès JR, Loiseau P, Bonvalet J, Tarisien M, d'Humières E, et al. (2021) Over-critical sharp-gradient plasma slab produced by the collision of laser-induced blast-waves in a gas jet: Application to high-energy proton acceleration. Physics of Plasmas 28: 023103.
19. Yang H (2024) Improving prediction accuracy of laser-induced shock wave velocity prediction using neural networks. Scientific Reports 14: 13576.
20. Dreze C, Demers Y, Gagné JM (1982) Mechanistic study of the optogalvanic effect in a hollow-cathode discharge. Journal of the Optical Society of America 72: 912-917.
21. Sharma RC (1995) Laser photoacoustic and laser optogalvanic spectroscopy of atoms and molecule. Ph D thesis, Department of physics BHU Varanasi (1995).
22. Sharma RC, Kundu T, Thakur SN (1998) Laser optogalvanic spectroscopy of argon in the wavelength region 605–740 nm. Pramana 50: 419-432.
23. Torres C, Reyes PG, Castillo F, Martínez H (2012) Paschen law for argon glow discharge. In Journal of Physics: Conference Series 370: 012067.
24. Racah G (1942) On a new type of vector coupling in complex spectra. Physical Review 61: 537.
25. Nestor JR (1982) Optogalvanic spectra of neon and argon in glow discharge lamps. Applied Optics 21: 4154-4157.
26. Su MC, Ortiz SR, Monts DL (1987) Optogalvanic wavelength calibration in the 555–575 nm region using argon. Optics communications 61: 257-260.
27. Reddy BR., Venkateswarlu P, George MC (1989) Penning type of ionizing energy transfer collisions in a Hg-Ar discharge detected by the optogalvanic effect. Optics communications 73: 117-120.
28. Moore CE (1971) Atomic energy levels, NSRDS-NBS 35. National Bureau of Standard, Washington, DC.
29. Miyabe M, Sato Y, Wakaida I, Terabayashi R, Sonnenschein V, et al. (2021) Odd-parity autoionizing levels of uranium observed by two-color two-step photoionization optogalvanic spectroscopy. Journal of Physics B: Atomic, Molecular and Optical Physics 54: 145003.
30. Kumar PK, Srikanth G (2021) Frequency and amplitude modulation of a cw-dye laser for measuring hyperfine frequency separations in optogalvanic spectra of 139La I. Applied Optics 60: 3430-3439.
31. Bickel GA, Innes KK (1985) Near infrared and visible two-photon transitions in the optogalvanic spectrum of neon. Applied optics 24: 3620-3624.
32. Thakur SN, Narayanan K (1992) Rydberg series in the visible two-photon optogalvanic spectrum of neon. Optics communications 94: 59-65.
33. Begemann MH, Saykally RJ (1982) Color center laser optogalvanic spectroscopy of lithium, barium, neon and argon Rydberg states in hollow cathode discharges. Optics Communications 40: 277-282.
34. Sobolewski ŁM, Kwela J, Windholz L (2021) Optogalvanic spectroscopy of the Zeeman structure of argon energy levels close to the ionization limit. Journal of Quantitative Spectroscopy and Radiative Transfer 272: 107778.
35. Alnama K, Jazmati A (2021) On the Time Resolved Optogalvanic Spectroscopy of Neon in a Hollow Cathode Discharge. Journal of Nano-and Electronic Physics 13: 1-6.
36. Shuker R, Ben Amar A, Erez G (1983) Theoretical and experimental study of the resonant optogalvanic effect in neon discharges. Le Journal de Physique Colloques 44: C7-C35.
37. Chen JR, Suen TH, Kung CY, Wang LB, Liu YW (2022) High stability multiple-frequency cavity locking based on Doppler-free optogalvanic Calcium ion spectroscopy. Optics Express 30: 28170-28181.
38. Biraben F, Giacobino E, Grynberg G (1975) Doppler-free two-photon spectroscopy of neon. Physical Review A 12: 2444.
39. Khwairakpam OS, Mariotti E, Scarpa D, Nicolosi P, Khanbekyan A, et al. (2022) Laser photo-ionization study of nat Ag using opto-galvanic signal at SPES offline laser lab. Journal of Instrumentation 17: C12009.
40. Kim JB, Kawamura K, Choi YW, Bowden MD, Muraoka K, et al. (1998) A method to measure electric field strengths in an argon glow discharge plasma using laser spectroscopy. IEEE transactions on plasma science 26: 1556-1561.
41. Piracha NK, Baig MA, Khan SH, Suleman B (1997) Two-photon optogalvanic spectra of argon: odd parity Rydberg states. Journal of Physics B: Atomic, Molecular and Optical Physics 30: 1151.
42. Koepke M (2024) Detection of Optogalvanic Spectra Using Driven Quasi-Periodic Oscillator Dynamics. Atoms 12: 42.
43. Sobolewski ŁM, Kwela J, Windholz L (2021) Optogalvanic spectroscopy of the Zeeman structure of argon energy levels close to the ionization limit. Journal of Quantitative Spectroscopy and Radiative Transfer 272: 107778.
44. Dos Santos JR, Bueno P, Jakutis J, Victor AR, Barreta LF, et al. (2023) Dysprosium optogalvanic spectroscopy in a hollow cathode lamp. Journal of the Optical Society of America B 40: 1141-1147.
45. Green RB, Keller RA, Luther GG, Schenck PK, Travis JC (1976) Galvanic detection of optical absorptions in a gas discharge. Applied Physics Letters 29: 727-729.
46. Lu H, Varvarezos L, Nicolosi P, Andrighetto A, Scarpa D, et al. (2022) Laser double optical resonance excitation-ionization of Mo with optogalvanic detection. Physica Scripta 97: 024004.
47. Bueno P, Sbampato ME, Neri JW, Neto JJ, Barreta LFN, et al. (2021) Simultaneous intermodulated optogalvanic spectroscopy and laser induced fluorescence in an erbium hollow cathode lamp. Spectrochimica Acta Part B: Atomic Spectroscopy 181: 106220.
48. Windholz L (2024) Comparison of Optogalvanic and Laser-Induced Fluorescence Spectroscopy. In Photonics 11: 279.
49. Sobolewski ŁM, Rathi S, Sharma L, Windholz L, Kwela J (2024) Laser optogalvanic spectroscopy of lead lines Isotope shifts and hyperfine structure studies. Journal of Quantitative Spectroscopy and Radiative Transfer 316: 108901.